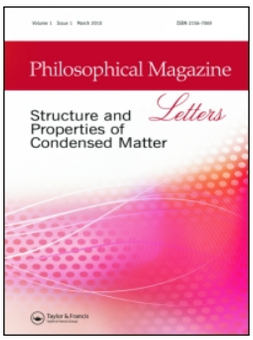

Philosophical Magazine Letters

ISSN: 0950-0839 (Print) 1362-3036 (Online) Journal homepage: http://www.tandfonline.com/loi/tphl20

A comparative study of Sm networks in Al-10 at.%Sm glass and associated crystalline phases

Xiaobao Lv, Zhuo Ye, Yang Sun, Feng Zhang, Lin Yang, Zijing Lin, Cai-Zhuang Wang & Kai-Ming Ho

To cite this article: Xiaobao Lv, Zhuo Ye, Yang Sun, Feng Zhang, Lin Yang, Zijing Lin, Cai-Zhuang Wang & Kai-Ming Ho (2018) A comparative study of Sm networks in Al-10 at.%Sm glass and associated crystalline phases, Philosophical Magazine Letters, 98:1, 27-37, DOI: 10.1080/09500839.2018.1447157

To link to this article: https://doi.org/10.1080/09500839.2018.1447157

Published online: 03 Apr 2018.

PHILOSOPHICAL MAGAZINE LETTERS, 2018
VOL. 98, NO. 1, 27–37
https://doi.org/10.1080/09500839.2018.1447157

Taylor & Francis
Taylor & Francis Group

A comparative study of Sm networks in Al-10 at.%Sm glass and associated crystalline phases

Xiaobao Lv[a,b], Zhuo Ye[b], Yang Sun[b], Feng Zhang[b], Lin Yang[b,c], Zijing Lin[a,d], Cai-Zhuang Wang[b] and Kai-Ming Ho[b,c,d]

[a]CAS Key Laboratory of Strongly-Coupled Quantum Matter Physics, Department of Physics, University of Science and Technology of China, Hefei, China; [b]Ames Laboratory, US Department of Energy, Ames, IA, USA; [c]Department of Physics, Iowa State University, Ames, IA, USA; [d]Hefei National Laboratory for Physical Sciences at the Microscale and Department of Physics, University of Science and Technology of China, Hefei, China

ABSTRACT

The Al–Sm system is selected as a model system to study the transition process from liquid and amorphous to crystalline states. In recent work, we have shown that, in addition to long-range translational periodicity, crystal structures display well-defined short-range local atomic packing motifs that transcends liquid, amorphous and crystalline states. In this paper, we investigate the longer range spatial packing of these short-range motifs by studying the interconnections of Sm–Sm networks in different amorphous and crystalline samples obtained from molecular dynamics simulations. In our analysis, we concentrate on Sm–Sm distances in the range ~5.0–7.2 Å, corresponding to Sm atoms in the second and third shells of Sm-centred clusters. We discover a number of empirical rules characterising the evolution of Sm networks from the liquid and amorphous states to associated metastable crystalline phases experimentally observed in the initial stages of devitrification of different amorphous samples. As direct simulation of glass formation is difficult because of the vast difference between experimental quench rates and what is achievable on the computer, we hope these rules will be helpful in building a better picture of structural evolution during glass formation as well as a more detailed description of phase selection and growth during devitrification.

ARTICLE HISTORY
Received 2 November 2017
Accepted 9 February 2018

KEYWORDS
Al–Sm system; liquid, amorphous, glassy and crystalline states; molecular dynamics simulations; medium-range order

1. Introduction

Amorphous metal structures have higher tensile yield strengths, higher elastic strain limits and special magnetic properties compared to traditional polycrystalline metal [1–3]. These amorphous metals can be synthesised by driving the alloy system far from equilibrium using rapid solidification. When heated, the glasses often devitrify into novel and complex metastable crystalline phases not observed in traditional synthesis. These crystal structures have well-defined structural orders in terms of both local atomic packing and long-range translational periodicity. It is generally believed that there is some correlation between the

CONTACT Zhuo Ye zye@iastate.edu; Kai-Ming Ho kmh@iastate.edu

structural order in amorphous glasses and these devitrified crystalline structures. However, the 'hidden' features that steer the initial transition from the amorphous to the crystalline state are still not clear.

In this work, in an attempt to clarify these 'hidden' features we select one of the Al-rich alloys (Al–Sm system) as an example to study the transition process from liquid and amorphous to crystalline states. The Al–Sm alloy is a model system for which the structural characteristics of the amorphous state allow the realisation of several intermediate metastable phases through path-dependent devitrification [4–8]. As reported in our recent work [8,9], a specific Sm-centered first-shell atomic packing motif is found to transcend undercooled liquids, glasses and crystalline phases that precipitate directly from glasses. The ε-$Al_{60}Sm_{11}$ and θ-Al_5Sm phases share the same 3–6–6–1 motif as the dominant motif observed in the amorphous phase [7,8]. Another motif, designated 1–6–6–6–1, is shared by the ε-$Al_{60}Sm_{11}$ and the η-$Al_{41}Sm_5$ phases [10]. While our studies have shown that the short-range order (SRO) plays an important role in phase selection during devitrification processes, the question remains, as to why different crystalline phases with the same SRO are selected through different devitrification processing methods. To answer this question, we extend our investigation to study the longer range spatial arrangement of the system, i.e. the medium-range order (MRO).

Recognising structural orders in amorphous glasses where long-range translational symmetry is absent has long been a challenging problem. While clear elements of SRO in terms of atomic packing motifs have been identified and analysed [9,11,12], limited work focusing on MRO in amorphous metals has been reported [13–15]. Amorphous metals do not present explicit networks as in network glasses, so that the definition and quantitative description of MRO is an even harder problem than for SRO. Different packing schemes such as cluster packing on a face-centered cubic lattice [13] and on an icosahedral packing [14] have been proposed. While these studies have advanced our comprehension of the MRO in selected systems, we want a faster and more general approach that can bridge the evolution between the amorphous glasses and their devitrified crystalline phases. Such an approach is especially attractive since our previous observation of common SRO supports a structural-hierarchy picture of complex phase selections from amorphous alloys where nascent short-range cluster motifs in the undercooled liquid or amorphous state rearrange their long-range packing to yield the devitrified crystal phases.

Taking into account the large size disparity and affinity between Al and Sm atoms, the dominant MRO in the Al-10%Sm system is most easily visualised by focusing on the solute Sm network. Al atoms in the system also have an influence on the Sm MRO. The Al MRO is intricately linked to the Sm MRO, but much more complicated to analyse. Using molecular dynamics (MD) simulations, we obtained atomic configurations of Al–Sm systems in different states: for disordered states we have Al-10%Sm undercooled liquids, and also glasses obtained by sub-Tg MD annealing under different periods of simulations; for crystalline states we consider three devitrified phases, namely ε-$Al_{60}Sm_{11}$, θ-Al_5Sm and η-$Al_{41}Sm_5$ [7,8,10], that are grown in computer simulations where ideal stoichiometric templates are simulated in contact with undercooled Al-10%Sm liquids. The $Al_{11}Sm_3$ equilibrium phase is not included here, because no similarity is found between $Al_{11}Sm_3$ and liquid in terms of short-range order [9]. Experimentally, these crystalline phases form from constant-heating-rate (CHR) devitrification of Al–Sm glass produced by either melt-spinning or magneton sputtering. The ε-phase [8] is the first crystallised phase that forms upon CHR heating

of melt spun Al-10.2%Sm ribbons with a near polymorphic transition. The composition of the stoichiometric ε-$Al_{60}Sm_{11}$ phase is different from that of Al-10%Sm alloy. The ε-phase is tolerant of Al/Sm anti-site defects. As a result, the crystallised structure has the same composition of the initial alloy. The as-grown crystal structure from MD simulation also has Al/Sm anti-site defects and has the same composition as the initial alloy, which is consistent with experiments. The θ-phase [7] is the first devitrified phase along from the magneton-sputtered Al-10%Sm thin film after it separates into Al-rich and Sm-rich regions. Face-centered cubic (fcc) Al appears together with the θ-phase as the composition of the θ-phase is different from that of the amorphous alloy. The θ-phase is also the first crystallised phase with fcc-Al from Al–14.1%Sm ribbons. The η-phase [10] appears as a small fraction along with the ε-phase and fcc-Al from melt-spun Al–9.7%Sm ribbons. It grows to a larger fraction (~35 wt.%) with an isothermal hold just before the crystallisation of the ε-phase. As crystalline structures formed from highly driven structural transitions often contain a substantial number of crystal-chemical defects, we perform large-scale MD simulations to 'grow' crystalline structures from undercooled liquids and seeds of stoichiometric crystals. Comparison between experimental XRD patterns and those computed from the simulated crystals show excellent agreement, with no additional fitting of atom positions or site-occupancies [7,8]. This agreement indicates that the simulated crystal growth is realistic and can be used for analysis of MRO.

The interfacial energy is a very important factor for nucleation. However, investigation of interfacial energy is beyond the scope of this work, and the current MD simulations do not yield any information on it. Other interface properties, such as the interfacial mobility and growth kinetics, are investigated elsewhere [16].

2. Computational details

We investigate the MRO of the following MD simulated samples: (1) amorphous Al-10%Sm undercooled liquids annealed for 2.5 ns at 800 K; (2) amorphous Al-10%Sm glasses annealed for 0.8 and 50 μs at 650 K; (3) ε-$Al_{60}Sm_{11}$, stoichiometric crystals and grown structures from Al-10%Sm undercooled liquids; (4) θ-Al_5Sm, stoichiometric crystals and grown structures; (5) η-$Al_{41}Sm_5$, stoichiometric crystals and grown structures.

Al-10 at.%Sm undercooled liquid and glass models are generated by large-scale MD simulations. All the MD simulations in this work were performed using the LAMMPS code [17]. A classical Embedded-Atom Method (EAM) potential in Finnis–Sinclair (FS) form [18] is used to expedite the MD simulations. As previously shown [6,19], this FS potential fitted to *first principles* calculation data gives, in general, a satisfactory estimation of the relative thermodynamic stability of the known stable and meta-stable phases. We have used the same potential to successfully localise the ε-, θ- and η-phases [7,8]. The initial liquid, containing 4500 Al and 500 Sm atoms, are held at 2000 K for 2.5 ns to reach equilibrium. Then, the liquid is continuously cooled down with a constant rate 10^{10} K/s to 800 K, which is below the melting temperature. After holding the sample at 800 K for 2.5 ns, we obtained the equilibrated undercooled liquid model. Then, the undercooled liquid is further cooled to 650 K, which is below the glass transition temperature $T_g = 693$ K [19]. After that, the sample is annealed isothermally at 650 K for 0.8 μs and 50 μs, respectively. Finally, these two glass samples annealed at sub-T_g for different time, are cooled to 300 K. Previous studies have demonstrated that annealing glass below, but close to, the glass transition temperature

can help structural relaxations in the simulation [20,21]. The liquid sample, as well as two glass models with different relaxation time are used for MRO comparison.

Large scale (∼ 3000 atoms) MD simulations were performed to study the liquid-to-crystalline transformations. The same classical FS potential [19] was used to expedite the MD simulations. The initial model contained the liquid Al-10%Sm alloy and a seed of ε-$Al_{60}Sm_{11}$, θ-Al_5Sm, or η-$Al_{41}Sm_5$ crystal [7,8]. Since MD simulations of crystal growth can be very computationally expensive, they were performed at an elevated temperature of 800 K to further expedite the transformation (devitrifications of the ε-, θ- and η-phases are experimentally observed at 470 K, 425 K, and 470 K, respectively). At 800 K, the crystal grows to fill the simulation domain within 280 ns for the ε-phase, 760 ns for the θ-phase, and 150 ns for the η-phase, respectively. Figure 1 shows the MD-simulated liquid-to-crystalline transformations for the ε-$Al_{60}Sm_{11}$ phase, as an example of growing crystalline structures from undercooled liquids.

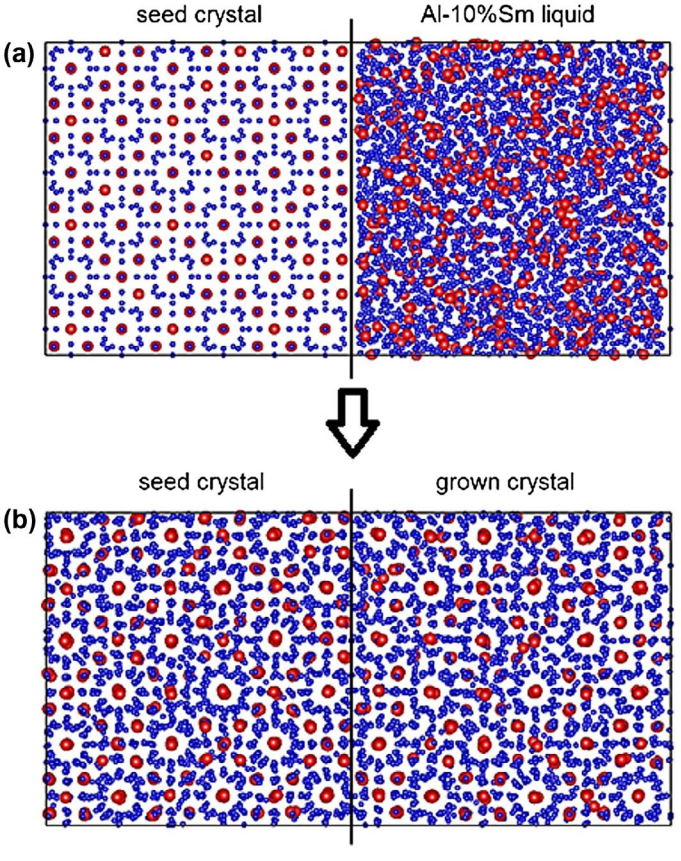

Figure 1. MD-simulated liquid-to-crystalline transformation for the ε-$Al_{60}Sm_{11}$ phase. (a) In the beginning, ε-$Al_{60}Sm_{11}$ crystal serves as a seed (left part) and contact with the undercooled Al-10%Sm liquids (right part) by a plane interface (the black vertical line in the middle). (b) After 280 ns MD simulation, the right part is fully grown to crystal with the help of the left seed part. In this figure, Sm and Al atoms are represented with red and blue colours, respectively.

3. Results and discussion

3.1. Sm–Sm partial pair correlation function

Sm–Sm partial pair correlation function (PPCF) was obtained from analysis of six different structures including the undercooled liquid, two glass structures annealed for 0.8 and 50 μs, respectively, and three crystal structures grown from undercooled liquids and stoichiometric crystalline seeds. The results are shown in Figure 2. Sm–Sm PPCFs of the 0.8 μs and 50 μs samples are essentially the same, indicating that medium-range structural orders in the glass do not experience significant changes even when the annealing time is extended to 50 μs even though there were significant changes in SRO. Thus, we use only the results of the 50 μs sample hereafter in this work. We note that, in general, time scale is a big challenge in MD simulations, and that a large difference of cooling rate exists between the simulated glasses ($\sim 10^{10}$ K/s) and real synthesised glasses ($\sim 10^{3} - 10^{6}$ K/s). Even with sub-T_g annealing to achieve an effective cooling rate of 6×10^{8} K/s [22], it is still several orders faster than experiments. 50 μs is probably not long enough to obtain a realistic low-energy glass structure. Comparing the Sm–Sm PPCFs of the undercooled liquid and the glass samples, as shown in Figure 1, the 1st peak in the short-bond region ($r < 4.5$ Å) is broader for the liquid sample than for the glass samples. Differences between glasses and the liquid are observed mainly in the medium-bond region (5.0 Å $< r <$ 7.2 Å), where the 2nd peak in the liquid sample is split into two sub peaks in the glass samples. The split of the 2nd peak is often observed in glass systems [15,23], indicating a refinement in the medium range Sm–Sm network from undercooled liquids to glasses. All of the three grown crystal samples have two major peaks in the same medium-bond region, although the peak positions vary depending on the different crystal structure. The PPCFs of the three grown crystals are more like that of the glass than the undercooled liquid in the medium-bond region.

In the following, we focus on the reorganisation of the Sm networks in this interesting medium range of $\sim 5.0 - 7.2$ Å for the six different samples. Although there are also

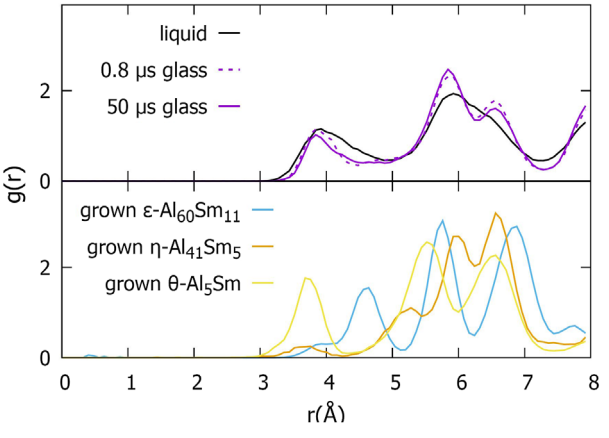

Figure 2. Partial pair correlation function (PPCF) of different Sm–Sm atom networks. The upper diagram is the PPCF of Sm in MD-simulated undercooled liquid (MD at 800 K) and glasses (MD at 650 K for 0.8 and 50 μs, respectively). The lower diagram is the PPCF of Sm in crystalline phases (they are ε-$Al_{60}Sm_{11}$, θ-Al_5Sm, and η-$Al_{41}Sm_5$ that are grown from liquid). The PPCF is averaged over 100 snapshots in the MD process of each sample.

noticeable changes occurring with Sm–Sm distances less than 5 Å, we found that Sm connections of such short lengths lead only to isolated dimers and o not to extended networks in the Al–Sm systems studied here. This is consistent with the strong preference of Sm atoms to be surrounded by Al atoms in the system on account of the much larger Al atom concentration and to the stronger chemical affinity of Sm atoms to Al atoms than to other Sm atoms. Thus, most Sm atoms are located in the 2nd and 3rd shell in a Sm-centered cluster.

3.2. Distribution of Sm coordination number

To analyse the interconnection of the different Sm networks, we tabulate the distribution of Sm neighbours in the 2nd and 3rd shell in the medium range of $\sim 5.0 - 7.2$ Å, and plot the population of Sm–Sm polyhedra with different coordinate numbers (CN) as a function of CN in Figure 3. The undercooled liquid and glass samples have only one broad peak, located at 6 and 7–8 coordination, respectively. The slightly larger CN in the glass indicates a denser medium-range clustering of Sm atoms in glasses. The CN of the three grown crystals are even larger. From low CN to high, the grown ε-$Al_{60}Sm_{11}$, η-$Al_{41}Sm_5$ and θ-Al_5Sm crystal structures peak at 7, 11 and 13. This represent a trend of increasing clustering of Sm atoms in the system as 2nd nearest neighbour or 3rd nearest neighbour positions. Experimentally the ε-phase forms directly from amorphous melt-spun Al-10.2%Sm ribbons in a nearly polymorphic transition with no chemical partitioning. From Figure 3, the CN of the ε-phase mostly resembles that of glass among the three crystal phases, which agrees with experimental observations. The fact that the η-phase has an overall higher CN than glasses and the ε-phase indicates that its MRO in the Sm–Sm network differs more than the ε-phase from glasses. It agrees with the experimental observations that a large fraction of the η-phase appears only with an isothermal hold just before the crystallisation of the ε-phase to slow down the formation of the ε-phase. The θ-phase precipitates from Sm-rich regions in magneton-sputtered Al-10%Sm thin films. The θ-phase is also the first crystallised phase from Al–14.1%Sm ribbons. It has the highest CN among all three grown crystals, which agrees with the fact that it forms from regions in which the Sm composition is higher than 10%. These observations suggest that the Sm–Sm network in the medium-range region may be

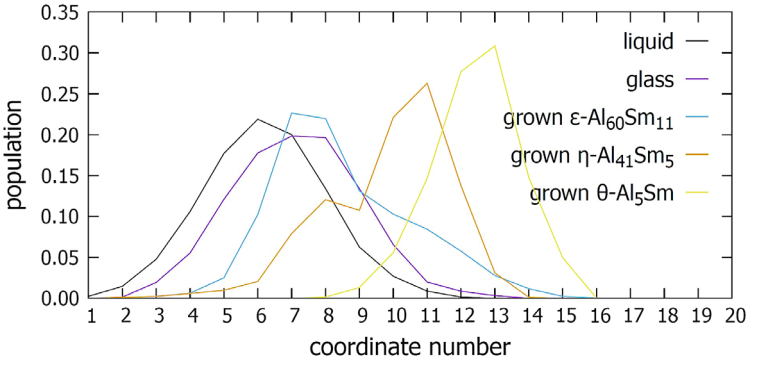

Figure 3. Distribution of the coordination number (CN) of Sm atom in different Sm–Sm networks. These are undercooled liquid, glass and three MD grown crystalline phases (ε-$Al_{60}Sm_{11}$, θ-Al_5Sm and η-$Al_{41}Sm_5$). The *x* axis represents the CN and the *y* axis represents the corresponding population of the Sm–Sm polyhedron with such CN in a specified phase.

a key step in the nucleation and growth of various metastable phases during devitrification. Further development of simplified network evolution models may be a fruitful approach to investigate the kinetic competition of various phase-selection devitrification pathways.

Figure 4a–e displays plots of the Sm–Sm polyhedra with peak CN as shown in Figure 3 in undercooled liquids, glasses and the grown structures of the three devitrified phases. As shown in Figure 4f, the stoichiometric ε-$Al_{60}Sm_{11}$ has two Wyckoff positions, 16f and 6b for Sm atoms with CN of 9 and 20, respectively. Both the experimental XRD and MD simulations show that the 16f site is evenly shared between Sm and Al [8], which reduces the CNs to 7.5 and 12. In Figure 3, the estimated CNs of 7.5 and 12 correspond to a major peak at $\sim 7-8$ and a shoulder at ~ 11, respectively. As shown in Figure 4g, the stoichiometric η-$Al_{41}Sm_5$ has two Wyckoff positions of 2b and 8 h for Sm atoms with CN of 12 and 13, respectively. In Figure 3, the CN is reduced to 8 and 11, indicating partial occupancy of Sm sites. As shown in Figure 4h, the stoichiometric θ-Al_5Sm has 1 Wyckoff position for Sm atoms with a CN of 15. The experimental XRD and MD simulations show that the Sm site is shared by Sm and Al with the Sm occupancy being $\sim 75-84\%$ [7], which will reduce the CN to $\sim 11-13$. It corresponds to the major peak at $\sim 12-13$ for the θ-phase in Figure 3.

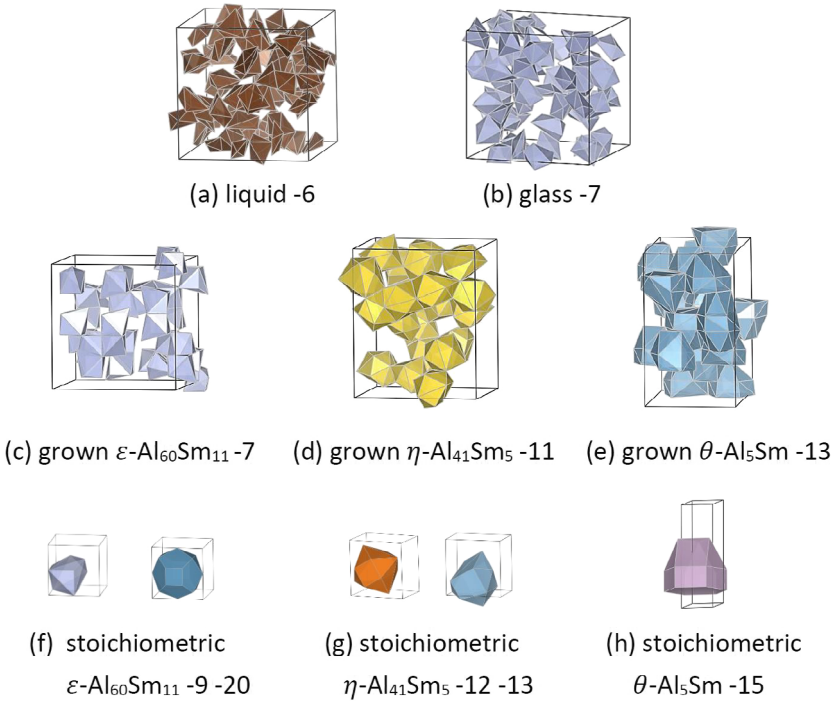

Figure 4. (a)–(e) The most favourable CN of Sm–Sm polyhedra in (a) undercooled liquids, (b) glasses, (c) grown ε-$Al_{60}Sm_{11}$, (d) grown η-$Al_{41}Sm_5$ and (e) grown θ-Al_5Sm. (f)–(g) The Sm–Sm polyhedra with different CN in stoichiometric crystals. The CN is shown at the end of each label with a hyphen ahead. Different colours of polyhedra represent different CN.

3.3. The angle distribution of Sm–Sm polyhedra

Using the CN one is not able to describe the shapes of different Sm–Sm polyhedra. To analyse the correlation of Sm–Sm polyhedra between undercooled liquids/glasses and the stoichiometric/grown crystal phases, we use the concept of renormalised angle sequence (RAS) to study the angle distribution of Sm–Sm polyhedra in different states. The RAS concept was first introduced for the Fe-P networks in $LiFePO_4$ crystals in our previous work [24]. Basically, it reduces the number of bond angles in a polyhedra to only two average angles, which represent large and small angles. In a Sm network, each Sm forms a polyhedron with its neighbouring Sm atoms. For example, a Sm atom with CN of N forms a polyhedron centred at itself with its N neighbour Sm atoms. There are N neighbour–centre Sm bonds emanating from this Sm atom and $N(N-1)/2$ bond angles. All the bond angles are then compared to the average bond angle and divided into two groups. The group with angles above the average has a group average angle which is the larger value of the RAS, and the

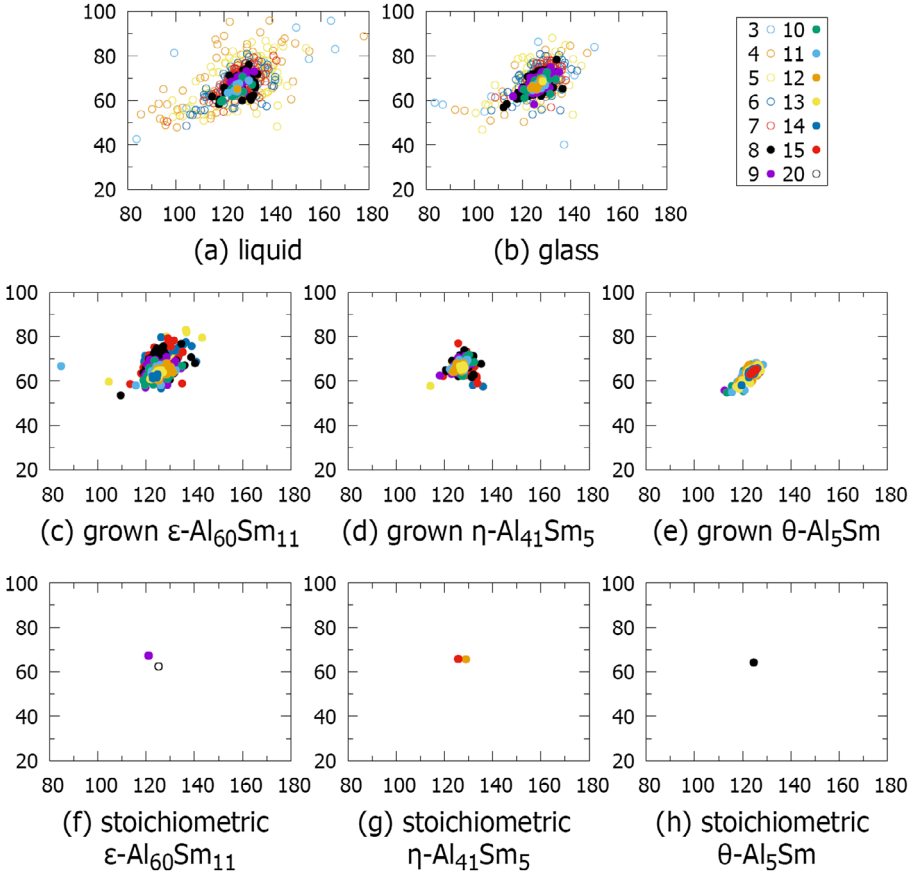

Figure 5. The RAS distribution of the eight structures in Figure 4. The *x* axis represents the large group-average angle and the *y* axis represents the small group-average angle of the Sm(neighbor)-Sm(centre)-Sm(neighbour) bond angles in a Sm–Sm polyhedron. Polyhedra with different CN are plotted with different colours.

group with angles below the average has a group average angle which is the smaller value of the RAS. Using the two RAS value as x and y axes, the RAS distribution is plotted in Figure 5.

As shown in Figure 5, the RAS distribution of Al-10%Sm glass is slightly more constrained than the undercooled liquid of the same composition. The RAS distribution of the three MD-grown crystals are even more constrained. Among them, the distribution of the grown ε-$Al_{60}Sm_{11}$ phase again mostly resembles that of glasses with the minor-CN Sm–Sm polyhedra disappearing. Compared to the grown ε-$Al_{60}Sm_{11}$ phase, the grown η-$Al_{41}Sm_5$ structures have a more compressed distribution, and the grown θ-Al_5Sm structures have the most compressed distribution, indicating that the Sm–Sm polyhedra shape varieties decrease, which can be directly seen in Figure 4d and e and in agreement with experimental results. It is interesting to see that the RAS distributions of all three grown structures are within the scope of liquids/glasses, indicating the structural hierarchy mechanism of complex phase selections from amorphous Al–Sm alloys. We also plot the distributions of stoichiometric crystals in Figure 5, which collapse to 1 or 2 points depending on how many Wyckoff positions of Sm sites there are. The grown crystals have lower coordination numbers than the stoichiometric crystals owing to the partial occupancies of Sm sites, as discussed above. Using the RAS concept, we are able to obtain a more compressive and intuitive view of Sm–Sm polyhedra shape changes in the devitrification process compared to the traditional angle distribution plot.

4. Conclusions

The MRO has been investigated in Sm networks of the Al-10%Sm system, including undercooled liquids, glasses, and three devitrified crystal phases. The Sm–Sm pair correlation function, the Sm coordination number distribution and the angular distribution of Sm–Sm polyhedra are studied. The characteristics of MRO in glasses lie between the undercooled liquid and the devitrified crystal phases. The MRO in the ε-$Al_{60}Sm_{11}$ phase is the most similar to the Al-10%Sm glass, which is consistent with the experimental observation that the ε-phase is the first crystallised phase from Al-10%Sm ribbon in a nearly polymorphic transformation with no chemical partitioning. We summarise several empirical rules that may be helpful in understanding the liquid-glass-crystal transformation in this system. The single peak of PPCF in undercooled liquids in the medium range splits into two peaks in glasses as well as in the devitrified crystal phases with moderate shifts. The CN of Sm–Sm polyhedra increase while the degree of shape varieties of Sm–Sm polyhedra decreases from undercooled liquids, glass to the devitrified crystals based on the CN and RAS analysis. Meanwhile, the RAS distributions of all three devitrified structures are within the scope of liquids/glasses, indicating the structural inheritance of crystallised phases from amorphous alloys.

Acknowledgements

Work at Ames Laboratory was supported by the US Department of Energy, Basic Energy Sciences, Division of Materials Science and Engineering, under Contract No. DE-AC02-07CH11358, including a grant of computer time at the National Energy Research Supercomputing Center (NERSC) in Berkeley, California. X.L. acknowledges support from USTC and the China Scholarship Council (File No. 201506340115). Z.L. acknowledges support from the National Natural Science Foundation of China (11374272, 11574284 & 11774324) and the Collaborative Innovation Center of Suzhou Nano Science and Technology. K.M.H. acknowledges support from the USTC Qian-Ren B (1000-Talents Program B) fund.

Disclosure statement

No potential conflict of interest was reported by the authors.

Funding

This work was supported by the China Scholarship Council [grant number 201506340115]; National Natural Science Foundation of China [grant number 11374272], [grant number 11574284], [grant number 11774324]. Work at Ames Laboratory was supported by the US Department of Energy, Basic Energy Sciences, Division of Materials Science and Engineering, under Contract No. DE-AC02-07CH11358.

ORCID

Xiaobao Lv http://orcid.org/0000-0003-0711-8936
Yang Sun http://orcid.org/0000-0002-4344-2920
Lin Yang http://orcid.org/0000-0003-0282-6116

References

[1] P. Chaudhari and D. Turnbull, Science 199 (1978) p.11.
[2] A.L. Greer, Science 267 (1995) p.1947.
[3] W.H. Wang, C. Dong and C.H. Shek, Mater. Sci. Eng. R: Rep. 44 (2004) p.45.
[4] P. Rizzi, M. Baricco, S. Borace and L. Battezzati, Mater. Sci. Eng. A 304–306 (2001) p.574.
[5] Y.E. Kalay, C. Yeager, L.S. Chumbley, M.J. Kramer and I.E. Anderson, J. Non-Cryst. Solids 356 (2010) p.1416.
[6] F. Zhang, I. McBrearty, R.T. Ott, E. Park, M.I. Mendelev, M.J. Kramer, C.Z. Wang and K.M. Ho, Scr. Mater. 81 (2014) p.32.
[7] Z. Ye, F. Zhang, Y. Sun, M.I. Mendelev, R.T. Ott, E. Park, M.F. Besser, M.J. Kramer, Z. Ding, C.Z. Wang and K.M. Ho, Appl. Phys. Lett. 106 (2015) p.101903.
[8] Z. Ye, F. Zhang, Y. Sun, M.C. Nguyen, M.I. Mendelev, R.T. Ott, E.S. Park, M. Besser, M.J. Kramer, Z.-J. Ding, C.-Z. Wang and K.-M. Ho, Phys. Rev. Mater. 1 (2017) p.055601.
[9] Y. Sun, F. Zhang, Z. Ye, Y. Zhang, X. Fang, Z. Ding, C.-Z. Wang, M.I. Mendelev, R.T. Ott, M.J. Kramer and K.-M. Ho, Sci. Rep. 6 (2016) p.23734.
[10] Z. Ye, F. Meng, F. Zhang, Y. Sun, L. Yang, S.H. Zhou, R.E. Napolitano, M.I. Mendelev, R.T. Ott, M.J. Kramer, C.Z. Wang, and K.M. Ho, preprint (2017), Available at arXiv, cond-mat.mtrl-sci/1712.09638.
[11] Y.Q. Cheng and E. Ma, Prog. Mater. Sci. 56 (2011) p.379.
[12] E. Ma, Nat. Mater. 14 (2015) p.547.
[13] D.B. Miracle, Nat. Mater. 3 (2004) p.697.
[14] H.W. Sheng, W.K. Luo, F.M. Alamgir, J.M. Bai and E. Ma, Nature 439 (2006) p.419.
[15] J. Ding, E. Ma, M. Asta and R.O. Ritchie, Sci. Rep. 5 (2015) p.17429.
[16] Y. Sun, Z. Ye, F. Zhang, Z. Jun Ding, C.-Z. Wang, M.J. Kramer and K.-M. Ho, Model. Simul. Mater. Sc. 26 (2018) p.015006.
[17] S. Plimpton, J Comput. Phys. 117 (1995) p.1.
[18] M.W. Finnis and J.E. Sinclair, Philos. Mag. A 50 (1984) p.45–55.
[19] M.I. Mendelev, F. Zhang, Z. Ye, Y. Sun, M.C. Nguyen, S.R. Wilson, C.Z. Wang and K.M. Ho, Model. Simul. Mater. Sc. 23 (2015) p.45013.
[20] F. Zhang, M.I. Mendelev, Y. Zhang, C.-Z. Wang, M.J. Kramer and K.-M. Ho, Appl. Phys. Lett. 104 (2014) p.061905.
[21] Y. Zhang, F. Zhang, C.Z. Wang, M.I. Mendelev, M.J. Kramer and K.M. Ho, Phys. Rev. B 91 (2015) p.064105.

[22] Y. Sun, Y. Zhang, F. Zhang, Z. Ye, Z. Ding, C.Z. Wang and K.M. Ho, J. Appl. Phys. 120 (2016) p.015901.
[23] X.J. Liu, Y. Xu, X. Hui, Z.P. Lu, F. Li, G.L. Chen, J. Lu and C.T. Liu, Phys. Rev. Lett. 105 (2010) p.155501.
[24] X. Lv, X. Zhao, S. Wu, P. Wu, Y. Sun, M.C. Nguyen, Y. Shi, Z. Lin, C.-Z. Wang and K.-M. Ho, J. Mater. Chem. A 5 (2017) p.14611.